

A 3-DIMENSIONAL RADIATIVE-TRANSFER HYPERSPECTRAL IMAGE SIMULATOR FOR ALGORITHM VALIDATION

S. C. Richtsmeier, A. Berk, L. S. Bernstein, and S. M. Adler-Golden
Spectral Sciences, Inc., 99 South Bedford Street, Suite 7, Burlington, MA 01803-5169

ABSTRACT

We are currently developing a high model fidelity HyperSpectral Image simulation software package. It is based on a Direct Simulation Monte Carlo approach for modeling 3D atmospheric radiative transport, as well as spatially inhomogeneous surfaces including surface BRDF effects. “Ground truth” is accurately known through input specification of surface and atmospheric properties, and it is practical to consider wide variations of these properties. Treating both land and ocean surfaces, 3D terrain, 3D surface objects, and effects of finite clouds with surface shadowing. The computed data cubes can serve both as a substitute for and a supplement to field validation data.

1. INTRODUCTION

Remote hyperspectral and multispectral imagery (HSI and MSI) of the Earth, typically acquired at wavelengths within the visible to near infrared region of around 400-2500 nm, has proven to be highly valuable for numerous applications, including mineral prospecting, environmental and land use monitoring, and military surveillance and reconnaissance. The quality of the data products depends critically on the accuracy of the atmospheric compensation, surface reflectance retrieval, detection/identification and other algorithms. Thus, there is a need for accurate, robust, and efficient means for algorithm validation. For this purpose, simulated imagery can provide a practical alternative to field measurements, which are typically expensive, time consuming, and impractical for covering the full range of anticipated atmospheric and surface conditions.

This paper describes the initial development of a first-principles, high-fidelity HSI/MSI image simulation capability that is based on a Direct Simulation Monte Carlo (DSMC) approach for modeling the 3D radiative transport, including light interactions with the atmosphere and object surfaces. With this approach, “ground truth” is accurately known through input specification of surface and atmospheric properties, and it is practical to consider wide variations in these properties. The method can treat land and ocean surfaces, effects of finite clouds, and other complex spatial effects, as indicated in Figure 1. The well-known drawback to the DSMC approach is the very large number of trial “photons” needed to achieve an accurate result, leading to very long computation times. However, recent advances in computing speed combined with convenient and affordable parallel processing systems are overcoming this limitation.

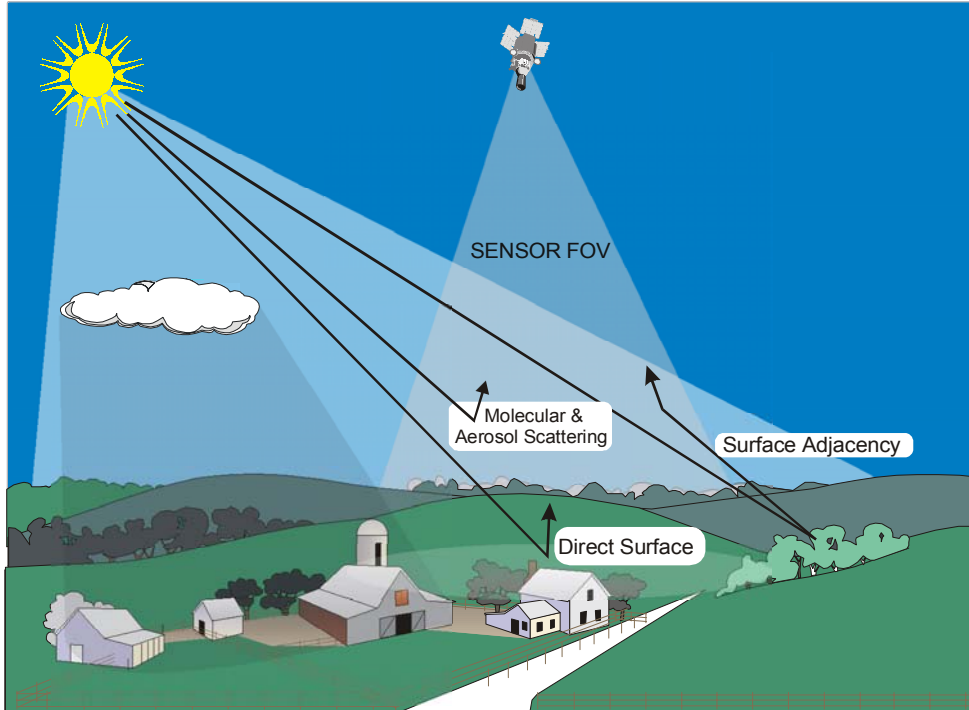


Figure 1. Important radiative transport effects for spectral image simulation, highlighting different trial photon trajectories.

The basic DSMC methodology is described in Section 2. Some initial results are presented in Sections 3 and 4, which include simulations of the effects of varying atmospheric visibility, the shadowing effects of a finite cloud, and validation of the multiple scattering results against “exact” calculations for homogeneous and vertically inhomogeneous clouds/aerosols.

2. MODEL DESCRIPTION

The current HSI/MSI data simulator incorporates all optical effects important for solar-illuminated scenes, including molecular and aerosol scattering and absorption, surface scattering with material-dependent bidirectional reflectance distribution functions (BRDFs), multiple scattering events, surface adjacency effects, and scattering and shading by clouds, for arbitrary solar illumination and sensor viewing geometries. As shown in Figure 2, the “world” of the simulation is a cube, 50 km on a side, that encloses a user-definable atmosphere containing molecular species, aerosols, and clouds, and a base representing the ground. The sensor spatial and spectral resolution, its location within the cube, and the viewing angle are also specified. The field of view (FOV) is a finely gridded inner region within the 50 km x 50 km ground area; in Figure 2, it is a 10 km square gridded with 1 m² pixels. Initial work has been performed assuming flat ground; however, the technique supports surface facets with arbitrary elevations and normals, which can be defined to describe 3D objects as well as terrain.

Surface reflectance properties within the FOV are assigned on a pixel-by-pixel basis. The area outside the FOV contributes to adjacency effects, *i.e.*, effects due to photons that reflect off the ground and scatter into the FOV.¹ This area is taken to be homogeneous, a simplification that should affect only the edges of the FOV, since the length scale of adjacency scattering is typically ~1 km or less. The reflectance functions for the ground materials are represented by a modified version of a Walthall surface BRDF.² This representation is computationally simple, is readily random-sampled, and is based on recent measurements and modeling of crops, soil, calibration surfaces, and roads.

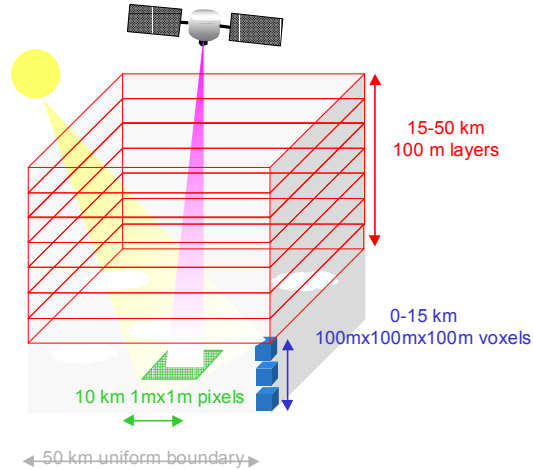


Figure 2. Elements of the scene definition in the simulation model.

Atmospheric information is stored as vertical profiles indexed to ground position. The atmosphere below 15 km altitude is divided into 100 m x 100 m x 100 m voxels, whose footprints cover the full 50 km square world. The atmosphere from 15 to 50 km is modeled as a single uniform profile with 100 m layers and no horizontal variability. The atmospheric profiles specify the altitude dependence of extinction cross-sections, scattering cross-sections, and densities for aerosols, clouds, and molecular species.

The image simulation is performed utilizing a backward Direct Simulation Monte Carlo (DSMC) radiative transport (RT) technique. (We use the term “backward” Monte Carlo as opposed to “forward” because photons are traced backwards along their trajectories from the sensor to the sun.) The major advantages of DSMC over other scattered radiance techniques are its simplicity, accuracy, and versatility, enabling rigorous modeling of complex 3D effects of clouds, shadowing, adjacency, terrain topography, etc. The major drawback of the DSMC technique is that it is computationally intensive. In the current model, the bulk of the computation time is spent calculating transmittances along the photon paths. These transmittance calculations have been optimized by using a fixed integration path length within altitude regions together with nearest-neighbor extinction coefficient data. This optimization, along with a physics-based sampling of the distributions influencing photon trajectories, make the process efficient enough to generate images at hyperspectral resolution.

In the backward DSMC method, many photons are launched toward the ground, their trajectories are followed, and their contributions to the apparent reflectance are accumulated as a function of pixel position to build up the scene at a given wavelength. Along these trajectories the photons may be scattered by molecules, aerosols, or clouds, they may be absorbed, or they may reflect from the ground. The mathematics of the Monte Carlo sampling of the different atmospheric and surface optical interaction distribution functions that describe the problem physics are discussed elsewhere³. A given photon may undergo multiple scattering events. A complete data cube is built up by performing the calculations for many different wavelengths.

Figure 3 provides a simplified flow chart of the calculation. The total apparent spectral reflectance is calculated by summing the atmospheric and surface scattering event contributions. The photon position and direction are initialized based on the sensor geometry, and a path optical depth is randomly selected. If the photon scatters within the atmosphere or off the ground, its contribution to the total solar scattered apparent reflectance is summed. The trajectory is terminated if the photon weight drops below a cutoff value or a maximum number of scattering events is reached. Otherwise, a new photon direction is randomly selected from the scattering distribution, and the photon trajectory continued. If the photon reaches the side or top boundary of the solution region, its trajectory is discontinued.

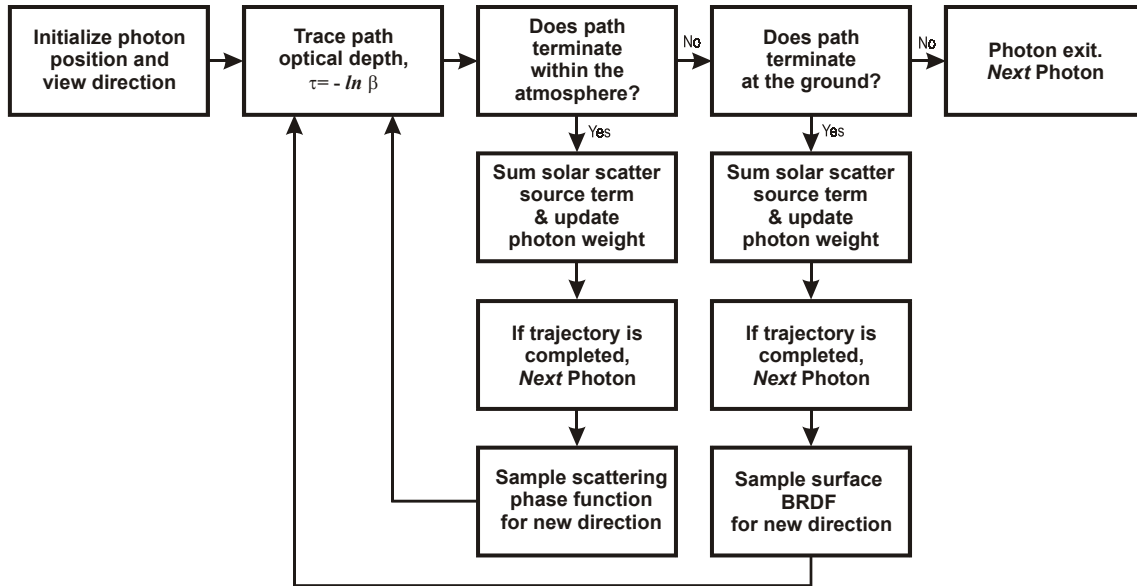


Figure 3. Photon trajectory flow chart.

Considerable effort was expended to optimize the computational efficiency of the code in order to make execution times reasonable. A typical full hyperspectral scene might involve 200 spectral channels and 10^6 image pixels. Using 10^4 photons per pixel per channel to achieve a 1% statistical accuracy, creating this data cube with the current DSMC RT model would require about 40 hrs of computational time on a 1 GHz microprocessor. This timing is for a simulation that includes Rayleigh, aerosol, and cloud scattering, and in which photons scatter 6 to 7 times on average. Individual pixels are calculated in a fraction of a second. Dramatic improvements in speed are anticipated with parallel computing systems. The DSMC method is highly parallelizable, since every photon trajectory and every wavelength is calculated independently of every other. Thus, even for a very large number of processors the computation time will decrease proportionally.

3. VALIDATION

The DSMC algorithm has been validated by comparing its predictions to closed-form solutions for simplified problems and to DISORT,⁴ a well-established scattering model that uses the discrete ordinate solution method. Figure 4 illustrates some of the results. On the left, the calculation of diffuse reflection for an isotropic scattering atmosphere with constant single scattering albedo is shown. There is an exact solution⁵. The sensor was modeled as nadir viewing for all the simulations and solar zenith angle was varied for two values of the single scattering albedo, $\omega = 0.800$ and $\omega = 0.975$. In all cases, the DSMC results converged to the closed form solutions as the number of photons increased. On the right of Figure 4, DSMC calculations are compared to calculations made using the DISORT model integrated with MODTRAN4.^{6,7} The multiple scattering contribution to the apparent reflectance for two ground albedo values is plotted as a function of visibility for a nadir viewing sensor at 20 km with MODTRAN Mid-Latitude Summer and Rural Aerosol Models defining the aerosol and Rayleigh optical depth profiles. The agreement provides confidence that the two models are solving the identical problems and reaching identical solutions.

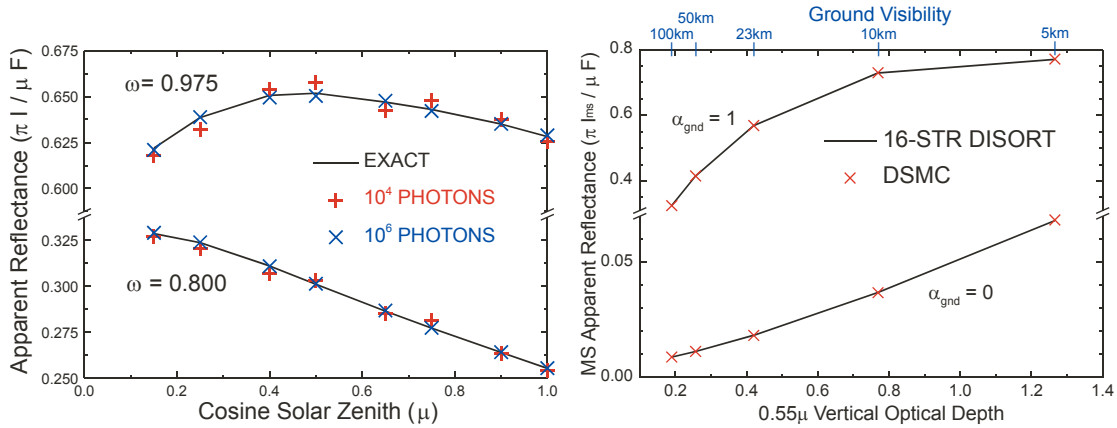


Figure 4. Results of calculations validating the DSMC algorithm. Comparison of the Monte Carlo simulation against the exact solution for an isotropic semi-infinite cloud is shown on the left. On the right, DSMC calculations of the multiple scattering contribution to the apparent reflectance are compared to 16-stream DISORT calculations.

4. IMAGE SIMULATION

A series of calculations were performed to demonstrate the utility of the simulation software for generating a realistic, high-spatial-resolution image. The scene construction was based on surface reflectance spectra retrieved from AVIRIS data taken over NASA’s Stennis Space Center. The retrievals were performed using the atmospheric compensation code of Adler-Golden *et al.*⁸; the results are in good agreement with ground truth spectra and radiosonde water vapor measurements. The atmosphere profiles are taken from MODTRAN’s mid-latitude summer model with a rural aerosol; a horizontally uniform atmosphere is assumed. The image size is 512 x 512 pixels, and a pixel size of 3 m, a little larger than that of the actual scene, is assumed. The sensor view is nadir and the solar zenith angle is taken as 30 deg. The calculations were performed at three wavelengths, denoted red, green, and blue (0.44, 0.55, and 0.65 μm , respectively). The area outside the FOV was assigned the average in-scene reflectance (0.073, 0.068, and 0.036, for red, green, and blue, respectively).

Figure 5 shows the effect of varying visibility on the apparent reflectance of the Stennis scene with the sensor at 20 km altitude. For comparison, the same scene is also shown without an intervening atmosphere. As the visibility is decreased from 100 to 23 to 5 km, the scene becomes increasingly hazy and the ground becomes more obscured.



Figure 5. Simulated effect of visibility on Stennis Space Center scene.

Figure 6 displays simulations for the same scene in which the visibility is fixed at 23 km, and the sensor altitude is varied from 20 km down to 2 km. The “no atmosphere” case is also included. With increasing altitude, the photons pass through more scattering layers and the apparent haziness increases.



Figure 6. Variation of sensor altitude for 23 km visibility Stennis scene.

The simulations in Figure 7 illustrate the adjacency effect, which is depicted in Figure 1. Since some photons reflected from portions of the surface not under direct observation can scatter into the sensor FOV, an observed pixel spectrum is in reality a blend of the line-of-sight in spectrum and a spatial averaged from the surrounding surface. For the simulation on the left in Figure 7, the surrounding spectral reflectance was taken as the scene average. For that on the right, this reflectance was increased by a factor of 5, resulting in a more hazy appearance.



Figure 7. Effect of boundary region reflectance on the apparent reflectance of the Stennis scene. The sensor is at 20 km and the solar zenith angle is 30 deg. At left, the boundary region reflectance is taken as the scene average. At right, the boundary reflectance is 5x higher.

5. CLOUD EFFECTS SIMULATION

A potentially valuable application of the DSMC simulations is in modeling cloudy scenes. For retrieving and interpreting reflectance under partly cloudy conditions, it is important to flag pixels that are contaminated by clouds. The development of efficient and accurate cloud masking algorithms is an active area of research,^{9,10} but is hindered in part by the inability to fully ground-truth the cloudy pixels in an image. This is essentially done by visual inspection, a subjective measure that can sometimes fail. The only objective and reliable way to validate cloud masking algorithms is through simulations, which provides the capability to insert clouds into a scene and vary key cloud and scenario attributes (*e.g.*, cloud altitude, illumination conditions) in a known manner.

To demonstrate DSMC cloud modeling with simple examples, we simulated a set of scenes containing a single cloud over a uniform surface. The cloud shape is depicted in Figure 9. It has a rectangular footprint and two regions of differing height (200 m and 100 m), giving it an "L" shape in side view. The optical thickness was chosen as 5 per km. The cloud base altitude was varied between 1.8 km and 7.8 km. The solar zenith angle was chosen as 30 degrees and the azimuth at 45 degrees relative to the long dimension of the cloud, such that the taller part of the cloud faces the sun and partly shadows the shorter part. Calculations were performed for four wavelengths, 650 nm (red = R), 550 nm (green = G), 440 nm (blue = B), and 935 nm (SWIR, in a water absorption band) and two different surfaces, dark vegetation (R, G, B reflectances of 0.015, 0.030, and 0.015, respectively) and light soil (R, G, B

reflectances of 0.34, 0.22, and 0.14, respectively). As a placeholder for an accurate correlated-k treatment that is currently under development, the water absorption at 935 nm was simulated using Beer's law with an appropriate average absorption coefficient. The atmosphere model is based on the MODTRAN Mid-Latitude Summer Atmosphere with a 23 km visibility rural haze.

Results from the simulations are shown in Figures 9 through 11. Figure 9 shows color and grayscale images of the vegetated scene. The cloud, at lower left, has an apparent reflectance ranging from around 0.2 to around 0.5; the darker areas occur at the edges of the cloud and in the self-shadow cast by the tall part of the cloud. The dark area at the upper right is the cloud's shadow on the ground. Due to illumination by the sky, the shadow has a slightly bluish color. In between the cloud and the ground shadow is a diffuse, faint shadow where illumination of the atmospheric aerosol is blocked; this shows up most clearly in the grayscale image, which is contrast-enhanced. This aerosol illumination is the same phenomenon that gives rise to the shafts of light often seen when sunlight passes through breaks between clouds.

Figure 10 shows the radiance along a diagonal cross section through the light soil scene. Most of the effects found in the vegetated scene also appear here, such as the ground shadow, the bluer color of the ground shadow (as evidenced by enhanced attenuation of the red and green wavelengths), and the wide range of brightness within the cloud from the self-shadowing and edge effects.

Figure 11 is similar to Figure 10 but shows the SWIR signal for various cloud altitudes. Note the reduction in the signal with decreasing altitude due to water absorption, and the very low signal coming from the ground. Note also the sharp edge at 24700 m, which corresponds to the edge of the tall part of the cloud.

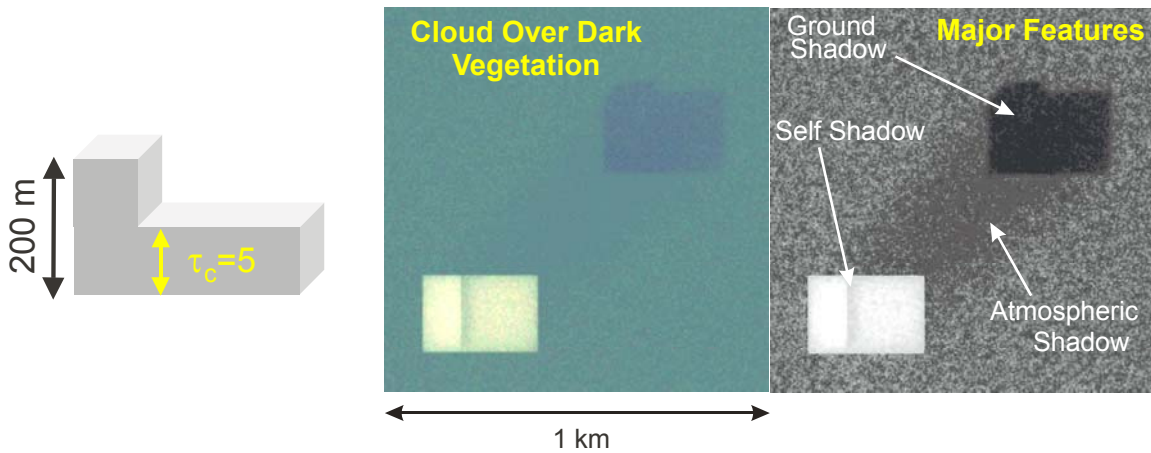


Figure 9. 3D Cloud Simulation.

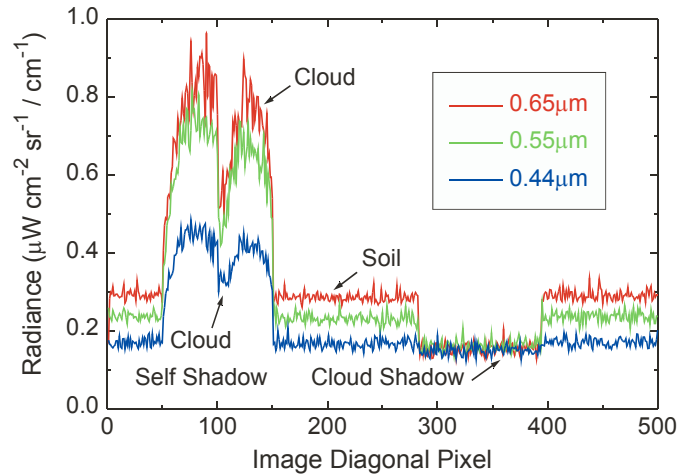


Figure 10. Radiance Along a Diagonal Cross-Section Through a Light Soil Scene.

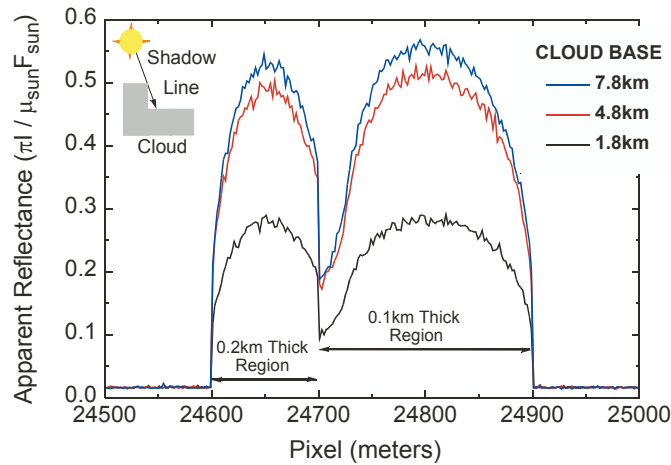


Figure 11. Apparent Reflectance at 935 nm for Various Cloud Altitudes

6. CONCLUSIONS

A practical, first-principles simulation model for hyperspectral or multispectral imagery has been developed based on a Direct Simulation Monte Carlo (DSMC) radiative transport approach. The code has been successfully validated through comparisons with exact scattering calculations, and its utility has been demonstrated in some initial applications to remote sensing problems. Reasonable computation times are obtained on a personal computer. The performance will continuously and rapidly improve as processor speeds increase and multi-processor (i.e., parallel processing) systems become commonplace. The current capabilities of the simulation code are unique and state-of-the-art, and are highlighted by the use of a rigorous radiative transport approach, a full 3D treatment of the atmosphere, including finite clouds, surface BRDFs, and a faceted surface description incorporating surface elevation and 3D objects. Further work is in progress to validate a correlated-k implementation of molecular absorption and to simulate complete hyperspectral data cubes.

ACKNOWLEDGMENT

The authors wish to acknowledge the support of NASA Stennis Space Center. This work is being performed under contract number NAS13-00025.

REFERENCES

1. Tanré, D., P. Y. Deschamps, P. Duhaut, and M. Herman, "Adjacency Effect Produced by the Atmospheric Scattering in Thematic Mapper Data," *J. Geophys. Res.* **92**, 12000 (1987).
2. Walthall, C. L., J.M. Norman, J. M. Wes, G. Campbell, and B. L. Blad, "Simple Equation to Approximate the Bidirectional Reflectance from Vegetation Canopies and Bare Soil Surfaces," *Appl. Optics* **24**:383-387 (1985).
3. Richtsmeier, S. C., L. S. Bernstein, A. Berk, and S. M. Adler-Golden, "A 3D Radiative-Transfer Hyperspectral Image Simulator for Algorithm Validation," Phase I Final Report NASA13-99014, SSI-TR-329, (1999).
4. Stamnes, K., S. -C. Tsay, W. Wiscombe, and K. Jayaweera, "Numerically Stable Algorithm for Discrete-Ordinate-Method Radiative Transfer in Multiple Scattering and Emitting Layered Media," *Applied Optics*, **27**, 2502-2509 (1988).
5. Chandrasekhar, S., (1960), *Radiative Transfer*, Dover Publications, Inc., New York, pp. 1-393.
6. Berk, A., L. S. Bernstein, and D.C. Robertson, "MODTRAN: A Moderate Resolution Model for LOWTRAN 7," GL-TR-89-0122, Geophysics Directorate, Phillips Laboratory, Hanscom AFB, MA 01731 (April 1989) ADA214337.
7. Berk, A., L. S. Bernstein, G. P. Anderson, P. K. Acharya, D. C. Robertson, J. H. Chetwynd and S. M. Adler-Golden, "MODTRAN Cloud and Multiple Scattering Upgrades with Application to AVIRIS," *Remote Sens. Environ.* **65**:367-375 (1998).
8. Adler-Golden, S. M., M.W. Matthew, L.S. Bernstein, R.Y. Levine, A. Berk, S.C. Richtsmeier, P.K. Acharya, G.P. Anderson, G. Felde, J. Gardner, M. Hoke, L.S. Jeong, B. Pukall, J. Mello, A. Ratkowski and H.-H. Burke, "Atmospheric Correction for Short-wave Spectral Imagery based on MODTRAN4," *SPIE Proceeding, Imaging Spectrometry V*, Volume 3753 (1999).
9. Ackerman, S. A., K. I. Strabala, W. P. Menzel, R. A. Frey, C. C. Moeller, and L. E. Gumley, "Discriminating Clear Sky from Clouds with MODIS," *J. Geophys. Res.*, **102**, 32141-32157 (1998).
10. Simpson, J. J., and J. R. Stitt, "A Procedure for the Detection and Removal of Cloud Shadow from AVHRR Data over Land," *IEEE Trans. Geosci. Remote Sens.*, **36**, 880-897 (1998).